ce/papers Proceedings in civil engineering

Ernst & Sohn A Wiley Brand

COMPARATIVE STUDY BETWEEN SHELL AND SOLID FINITE ELEMENT MODELS FOR STEEL JOINTS CHARACTERIZATION

J. Aguiar[a,*], F. Freire[a], A. F. Santos[a], F. Ljubinković[a], J. Conde[b], L. S. da Silva[a]

[a] *Universidade de Coimbra, ISISE, ARISE, Departamento de Engenharia Civil*
[b] *Universidad Politécnica de Madrid, Departamento de Física y Estructuras de Edificación*

Abstract. Solid and shell finite element models (FEM) are two commonly used possibilities to analyse the structural behaviour of steel joints. The choice between solid and shell models often comes down to a balance between computational resources and the level of detail required for the study. In this paper, a set of welded beam-column joints with hot-rolled open sections is studied using both modelling techniques. The joints' behaviour is assessed in terms of resistance and initial stiffness. An improved shell FEM is proposed. The results indicate that for the studied dataset, both techniques return comparable results. Hence, the use of shell FEM seems to be a possible alternative to solid FEM and can be efficiently used for the joint characterization.

1. Introduction

Joints are constituted by multiple elements that interact with each other which may lead to considerable complexity. Due to those factors (importance and complexity), the study of its behavior is an important research field. That increase in attention may be attributed to a change in the design philosophy in the United States of America after the 60's and the beginning of the 70's [1].

Solid and shell FEM are two commonly used possibilities to analyze the structural behavior of steel joints, for example, following the initial guidelines in [2] and [3]. The use of solid FEM may lead to more accurate results but requires the use of heavy computational resources while shell FEM may lead to less accurate results but saves computational resources when compared to solid [4] [5]

Given that a comprehensive comparison of the two modelling techniques for the steel joints is not yet reported in the literature, in this paper, such comparison is carried out using a sample of 20 one-sided-open section beam-to-column internal joints with negative bending moment applied on the extremity of the beam. The moment resistance of each joint is obtained using the 5% plastic strain criterion, as suggested by EN 1993-1-14 [6].

2. Numerical model definition

Numerical models were developed using the commercial software Abaqus® and its creation, running, and extraction of results was performed through Python scripts. A geometrically and materially nonlinear analysis with initial imperfections included (GMNIA) was chosen.

A buckling analysis (LBA) restricting the movements of the joint except for the column web panel was performed by applying only a concentrated moment in the free extremity of the beam, de-formed shape produced by the first buckling mode with an amplitude of $d_c/200$ was considered for the initial imperfections. The applied loading and boundary conditions are shown in Fig. 1.

The material used in numerical models is steel grade S275 for columns, whereas for the beam different steel grades are considered (S235, S275, S355, S460, S690). The theoretical elastic-perfectly plastic (EPPL) material law was selected, considering the converted true properties, as shown in Fig. 2. The Poisson's ratio v and the Young's modulus of steel E were taken as 0.3 and 210 GPa, respectively.

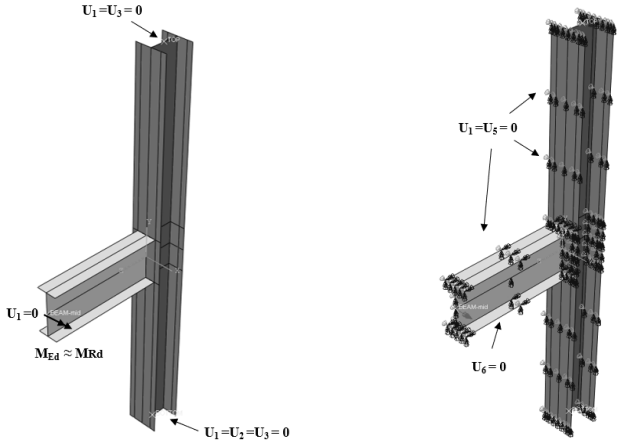

a) b)

Fig. 1: Loading and boundary conditions: a) GMNIA; b) LBA

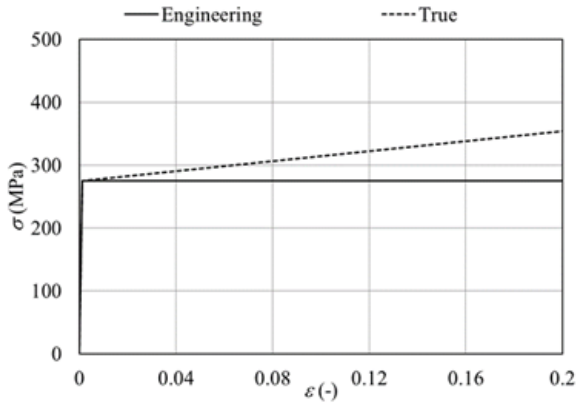

Fig. 2: Elastic-perfectly plastic (EPPL) material law

2.1 Shell modelling

For the shell models three different sections were considered to model the column, as represented in Fig. 3 (i) The first section, 'A', neglects the contribution of a thicker web-to-flange connection present in hot-rolled column profiles, defined by a radius r and therefore, does not have any change in CWP thickness along the web; (ii) The second section, 'B', tries to consider the contribution of the radius r by increasing the thickness of the web near the column web-to-

flange connection; (iii) the third section 'C' tries to consider the contribution of the radius *r* by adding two extra inclined shell elements in the column web-to-flange connection.

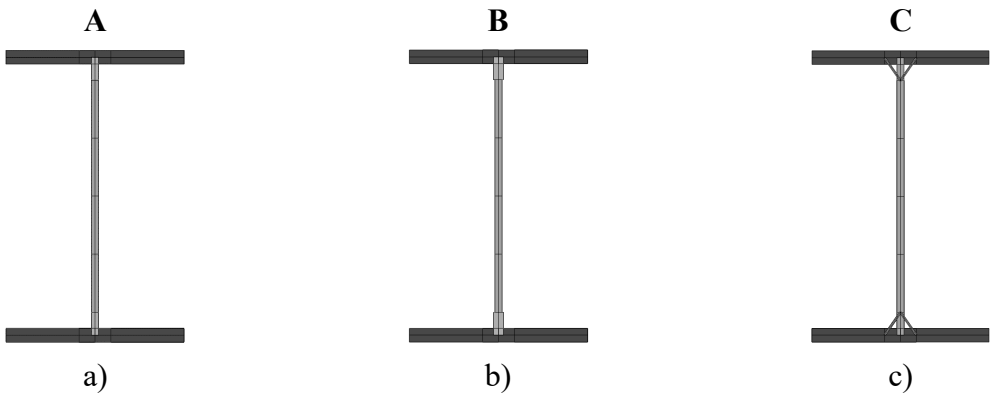

Fig. 3: Shell FEM sections. a) Section 'A', neglecting radius; b) Section 'B', increase in web thickness; c) Section 'C', inclined elements

For the increase of thickness in section "B" the cross-section is divided into three parts as shown in Fig. 4: (i) flanges AB and EF – with the thickness t_f and the width b_f; (ii) mid-web DH – with the thickness t_w and the width d_c; and (iii) web corners CD and GH – with the thickness t_{wr} and the l_r.

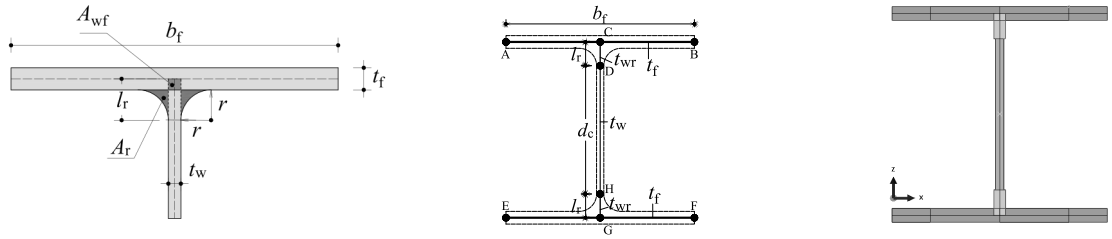

Fig. 4: Radius modelling by web thickness increase

where t_{wr} is the corrected thickness of the web corners, obtained as

$$t_{\mathrm{wr}} = t_{\mathrm{w}} + \frac{2A_{\mathrm{r}} - A_{\mathrm{wf}}}{l_{\mathrm{r}}}, \tag{1}$$

where A_r and A_{wf} are obtained as

$$A_{\mathrm{r}} = r^2\left[1 - \frac{\pi}{4}\right] \approx 0.214r^2, \tag{2}$$

$$A_{\mathrm{wf}} = \frac{t_{\mathrm{f}} t_{\mathrm{w}}}{2}, \tag{3}$$

and l_r is the length of the web corners, obtained as

$$l_{\mathrm{r}} = \frac{2r + t_f}{2}, \tag{4}$$

For section "C" the column root radius was considered by an analogy with the simulation of welds proposed by [7] and [4] using inclined shell elements linking the column web with its

flanges. Beyond the same cross-section divisions established in section 'B' 4 extra inclined elements were added: "Welds" LH, IH, JD, and KD. These elements have a thickness t_{weld} obtained as:

$$t_{weld} = \frac{A_{\mathrm{r}}}{\sqrt{{l_{\mathrm{r}}}^2 + {l_{\mathrm{rf}}}^2}}, \tag{5}$$

$$l_{\mathrm{rf}} = \frac{2r + t_{\mathrm{w}}}{2}, \tag{6}$$

A linear four-node shell element with reduced integration (S4R) is used for the model discretization. S4R was chosen because it is the general-purpose conventional shell element provided by Abaqus® [8]. Numerical models are discretized by four-node shell elements (S4R) with the reduced integration and 6 DOF per node, as a finite element commonly used for the discretization of thin plates and shell structures [7] [8] [9].

The size of the finite elements is determined based on a convergence study using section 'A' (for the model E1.2 from [7]), as shown in Table 1. It may be noticed that the increased FE leads to a decrease in bending resistance, and a delayed occurrence of the 5% plastic strain, as presented in Fig. 5. However, as may be seen the difference in moment resistance for the 5% plastic strain criterion (according to EN 1993-1-14) is smaller between meshes, which may be considered small in this study, so then, a 10 mm mesh could be considered sufficient to achieve numerical convergence with acceptable CPU time consumption. In addition, almost no difference may be found for initial stiffness between meshes.

Table 1: Difference in moment resistance based on the 5% plastic strain criterion

15 mm	10 mm	5 mm	15 to 10	15 to 5	10 to 5
M_{Rk} (kNm)			ΔM_{Rk} (%)		
239.9	230.5	220.3	3.9	8.2	4.4

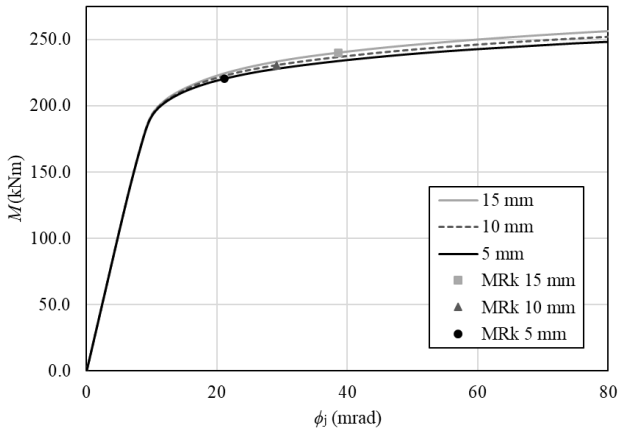

Fig. 5: Mesh sensitivity analysis moment-rotation curves

The physical contact between the beam and column face is modelled using tie constraint line by line.

2.2 Solid modelling

The FE solid model comprises a solid core region connected to shell parts using solid-shell couplings. The length of the members within the solid core part was defined as 1.25 times the height of the member for each side, indicated in Fig. 6.

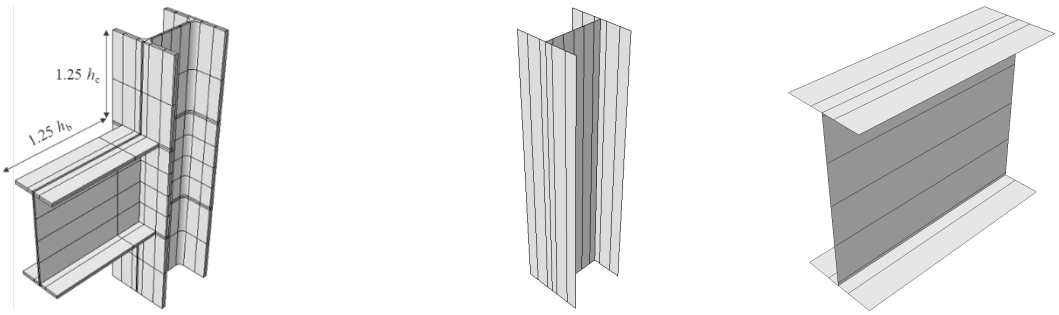

(a) (b) (c)

Fig. 6: Solid model description. (a) Solid core; (b) Column part (shell); c) Beam part (shell)

The influence of the mesh size and the element type were studied, leading to the following conclusions: the critical point for the plastic strain is highly dependent on the mesh size, i.e., the denser the mesh the smaller the moment/rotation corresponding to this critical point. On the other hand, the initial stiffness and the overall moment-rotation curve do not vary significantly either for the mesh size or the element type (see Fig. 7).

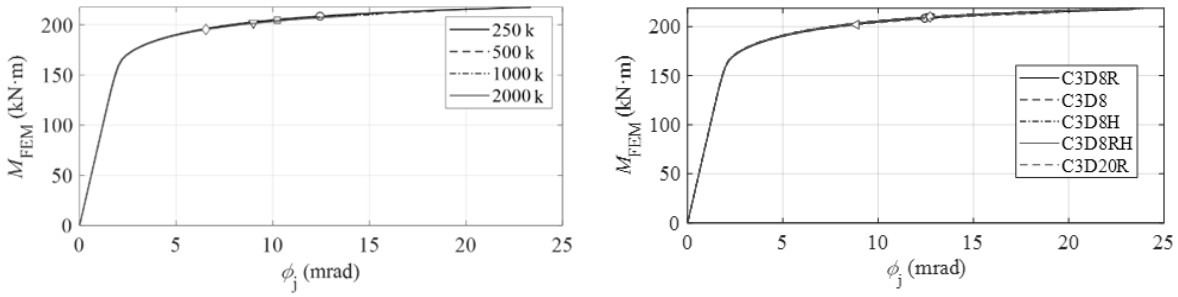

(a) (b)

Fig. 7: Mesh sensitivity analysis for FE solid models. (a) Mesh size; (b) Element type

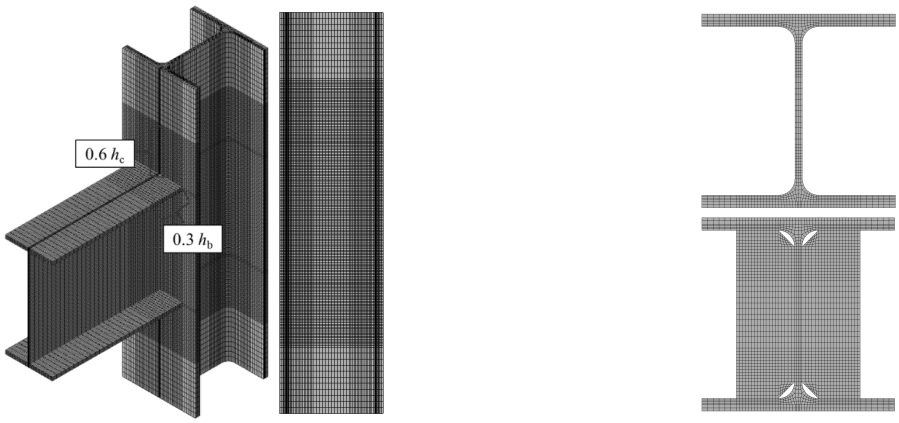

(a) (b)

Fig. 8: FE mesh for the solid core. (a) Refined region; (b) Cross section – unstiffened and stiffened

According to the results above, it can be observed that the initial stiffness and the overall moment-rotation curve do not vary significantly either for the mesh size or the element type. However, the critical point for the plastic strain is highly dependent on the mesh size, i.e., the denser the mesh the smaller the moment/rotation corresponding to this critical point. considering the computational time and storage required per model, the eight-node linear brick element with reduced integration

(C3D8R) was selected to model the solid core [10], and the mesh approximate size was interactively reduced until the mesh reached nearly 250,000 nodes, as presented in Fig. 8.

For the sake of simplification, the beam root radius was not modelled for shell parts. Full penetration butt welds were considered in the connection between the beam and the column. The region with greater stresses, i.e., the intersection between the beam and the column was kept with a denser mesh. This region called the "refined region", extends up to 0.3 h_b in the beam and 0.6 h_c in the column. The mesh was also optimized at the cross-section level, where regions with stress concentrations were more refined, e.g., close to the root radius.

2.3 Validation of FEM

The FE models were validated against experimental data, namely two welded joints from [7]. The experiments consisted of one-sided welded joints submitted to negative bending moment and without axial load applied in the column (for further information about geometrical characteristics and material properties see [7]).

The load-deflection curves that correlate the displacement on the tip of the beam (δ) and the applied moment were obtained for each model and compared with the experimental data as shown in Fig. 9.

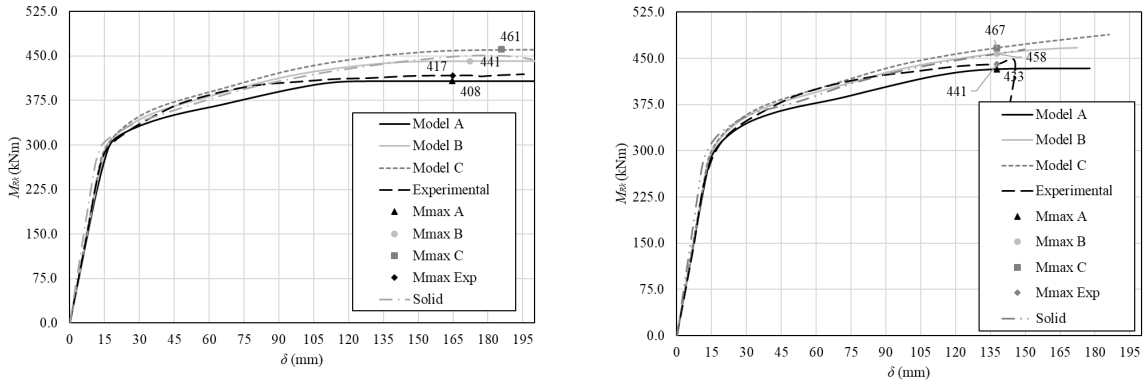

a) b)

Fig. 9: Moment-displacement curves. a) model E1.1; b) model E1.2

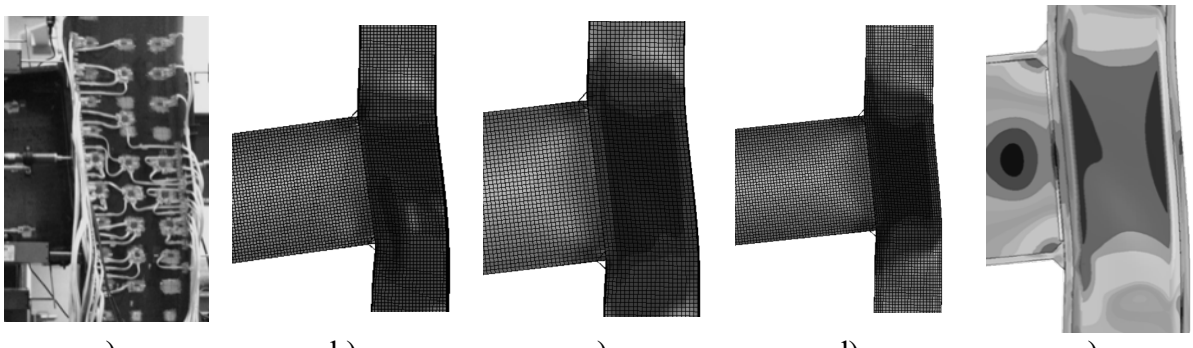

a) b) c) d) e)

Fig. 10: Deformed shapes. a) Test E1.2 [7] b) Model A; c) Model B; d) Model C; e) Solid

The comparisons show that there is a good agreement between experimental and numerical results for solid and shell FEM in terms of initial stiffness, resistance, and deformation. The largest differences in the M-δ curves were obtained for test S355 E1.2. However, it can be stated that the overall behavior of the joint is well captured, given the uncertainties from the experimental test. Finally, the true deformed shape of tests E1.1 and E1.2 seems to be like the deformed shape of the numerical models as may be seen in Fig. 10.

3. Parametric study

3.1 Definition of the sets considered

The study encompasses welded beam-to-column moment resisting joints between I and H-shaped hot-rolled open-section profiles. To use a sample that could be representative of the different columns used in common engineering practices. The columns were chosen based on the shear capacity of the column web panel and the column slenderness, as given by:

$$\lambda_{wp} = d_c / t_{wc}, \tag{7}$$

Based on the 7 columns, one set of 20 one-sided internal joints was created to have a representative sample of joint aspect ratios summarized in Table 2.

Table 2: Joint configuration and geometrical characteristics

nº	Column	Beam	*f*yc (MPa)	*f*yb (MPa)	zb1/*d*c	dc/twc	Lc (m)	Lb (m)
1	HE500A	HE400B	S275	S275	0.964	32.5	3.40	1.00
2	HE500A	HE600A	S275	S275	1.449	32.5	3.59	1.48
3	HE500A	HE800B	S275	S235	1.967	32.5	3.80	2.00
4	UC203x203x46	HE160A	S275	S235	0.887	22.4	3.15	0.38
5	UC203x203x46	IPE240	S275	S275	1.428	22.4	3.24	0.60
6	UC203x203x46	IPE330	S275	S235	1.976	22.4	3.33	0.83
7	HE280B	HE200B	S275	S275	0.944	18.7	3.20	0.50
8	HE280B	IPE300	S275	S355	1.476	18.7	3.30	0.75
9	HE280B	IPE400	S275	S275	1.972	18.7	3.40	1.00
10	HE140M	HE100B	S275	S690	0.978	7.1	3.10	0.25
11	HE140M	HE140B	S275	S355	1.391	7.1	3.14	0.35
12	HE140M	IPE200	S275	S460	2.082	7.1	3.20	0.50
13	UC305x305x240	HE260B	S275	S690	1.023	10.3	3.26	0.65
14	UC305x305x240	HE360B	S275	S275	1.423	10.3	3.36	0.90
15	UC305x305x240	IPE500	S275	S460	2.041	10.3	3.50	1.25
16	HE600x399	HE450M	S275	S355	0.901	16.2	4.48	1.20
17	HE600x399	HE700M	S275	S275	1.391	16.2	4.72	1.79
18	HE600x399	HE1000M	S275	S275	1.992	16.2	5.01	2.52
19	HE800B	HE700B	S275	S275	0.991	38.5	4.70	1.75
20	HE800B	HE1000B	S275	S275	1.430	38.5	5.00	2.50

The name for each model was created based on the following code:

0001-S-I-fy275-HE500A-AR103-N00

The first two numbers represent the number of the set, and the second two numbers represent the number of the joint, ‘I’ belongs to ‘internal’ followed by the yield strength of the steel of the column, the name of the profile of the column, the aspect ratio ‘AR’ and the axial force applied (referred in the percentage of the column plastic resistance).

3.2 Discussion of results

To control the plastic strain in the core of the column, 5 sets were created dividing the column profile into 5 areas. Following: S2FL back flanges of the beam, S1FL front flanges of the beam, S2RR back column radius area, S1RR front column radius area, WP column web panel, and Beam 1 beam of the join.

For every case, the moment-rotation curve was generated as shown in Fig. 11: Moment-rotation curves SET01. a) Shell FEM "C"; b) Solid FEM. Having the curves, the initial stiffness, and the characteristic value of the moment resistance criterion were calculated.

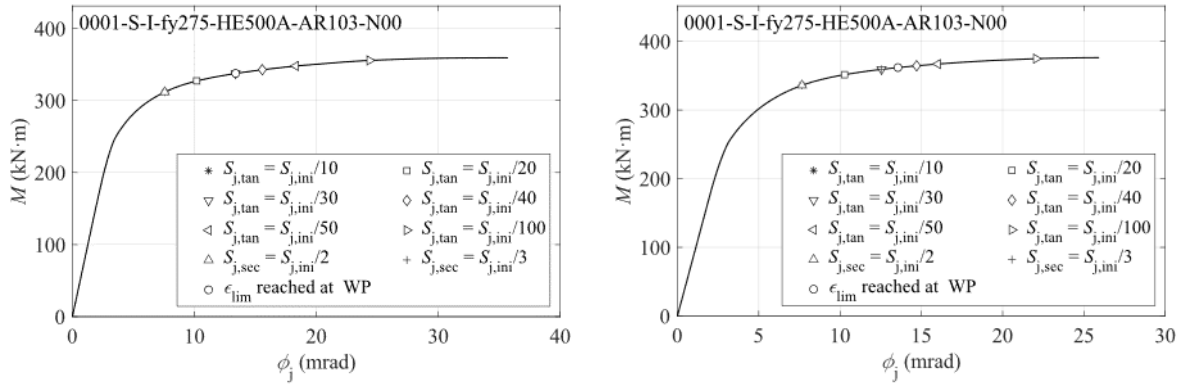

a) b)

Fig. 11: Moment-rotation curves SET01. a) Shell FEM "C"; b) Solid FEM

Table 3: Moment resistance and initial stiffness for solid and shell FEM

	M_R (kN·m)				$M_{R,Shell}$ / $M_{R,Solid}$			Sj,ini (kN·m/mrad)				Sj,ini,Shell / Sj,ini,Solid		
	Solid	"A"	"B"	"C"				Solid	"A"	"B"	"C"			
N°	[1]	[2]	[3]	[4]	[2]/[1]	[3]/[1]	[4]/[1]	[1]	[2]	[3]	[4]	[2]/[1]	[3]/[1]	[4]/[1]
1	361.8	296.3	332.5	337.7	0.82	0.92	0.93	88.2	77.0	81.1	83.6	0.87	0.92	0.95
2	575.7	492.6	531.6	539.3	0.86	0.92	0.94	153.6	139.4	146.3	150.3	0.91	0.95	0.98
3	828.6	719.9	762.7	773.4	0.87	0.92	0.93	225.8	208.1	218.0	222.5	0.92	0.97	0.99
4	35.5	32.3	33.5	36.3	0.91	0.94	1.02	7.4	6.7	6.8	7.1	0.91	0.91	0.95
5	58.0	53.2	55.1	58.7	0.92	0.95	1.01	15.1	14.2	14.3	14.9	0.94	0.95	0.99
6	81.7	75.8	77.0	82.2	0.93	0.94	1.01	21.9	21.2	21.2	22.0	0.97	0.97	1.00
7	110.4	93.0	109.1	111.1	0.84	0.99	1.01	22.5	18.5	20.0	21.0	0.82	0.89	0.93
8	164.1	146.5	168.3	171.4	0.89	1.03	1.04	40.7	35.8	38.6	40.7	0.88	0.95	1.00
9	223.3	197.5	222.6	222.6	0.88	1.00	1.00	57.7	51.8	55.7	57.9	0.90	0.96	1.00
10	44.1	49.0	41.8	49.8	1.11	0.95	1.13	9.2	8.4	7.7	8.9	0.91	0.84	0.97
11	60.9	61.8	55.2	63.8	1.01	0.91	1.05	13.3	11.8	10.9	12.5	0.88	0.82	0.93
12	81.4	85.7	78.2	87.2	1.05	0.96	1.07	21.0	20.3	18.5	21.5	0.97	0.88	1.02
13	421.4	399.9	335.2	406.7	0.95	0.80	0.97	84.0	76.2	71.3	79.7	0.91	0.85	0.95
14	588.9	540.4	460.6	553.2	0.92	0.78	0.94	128.2	116.5	108.4	121.1	0.91	0.85	0.94
15	783.2	759.9	661.8	780.9	0.97	0.85	1.00	198.3	191.8	177.5	199.1	0.97	0.90	1.00
16	1464.4	1286.6	1001.8	1329.2	0.88	0.68	0.91	348.1	310.6	289.4	321.7	0.89	0.83	0.92
17	2381.4	2071.6	1707.8	2172.7	0.87	0.72	0.91	610.4	569.0	531.3	587.4	0.93	0.87	0.96
18	3525.8	3082.2	2677.1	3169.1	0.87	0.76	0.90	898.0	867.2	812.3	891.9	0.97	0.90	0.99
19	1303.4	1058.6	1162.3	1179.6	0.81	0.89	0.91	359.1	328.0	333.3	346.9	0.91	0.93	0.97
20	2077.7	1761.8	1937.3	1912.3	0.85	0.93	0.92	589.5	556.0	564.2	583.4	0.94	0.96	0.99

All the results of the study are summarized in Table 3. Based on these results, it may be observed that between different shell FEM (B or C and A) the higher differences in moment resistance occurs for cases 10 to 18 for model B. Model B shows systematically lower resistances than model A (with a minimum of 22% lower for SET01). A possible explanation for this can be found in the formulation of section B, where the area resulting from the overlap of web and flange shell elements is considered and discounted. For cases 10 to 18, the column profiles have thick flanges and therefore, the discount of the overlap area leads, in fact, to a decrease and not an increase in web thickness for the root-radius zone compared to the actual web thickness.

On the other hand, for the remaining cases, both models C and B show systematically higher or equal moment resistances than model A. Model C leads to a mean moment resistance increase of 7.8% with Std. deviations below 0.06. Model C also presents systematically higher moment resistances than model B for all cases. Namely, a mean 11% increase for SET01 and maximum values that are 33% higher.

Comparing the results provided by the different shell models, the initial stiffness seems to have a relatively small variation of the mean initial stiffness between models A, B, and C.

Model B leads to a mean initial stiffness 1.1% lower than model A for SET01 while Model C leads to a mean initial stiffness 6.3% higher than model A.

When compared to solid FEM the moment resistance obtained by shell FEM may be lower in mean values. Namely, 8.92, 10.85 and 2.08% lower for "A", "B" and "C" models. A similar tendency may be observed for the initial stiffness, with the mean values provided by shell FEM lower compared to solid FEM. Namely, the mean values for the initial stiffness provided by the shell FEM "A", "B" and "C" are 8.45, 9.5,8 and 2.77% lower compared to solid.

The standard deviation seems to be under 0.1 for all shell FEM compared to solid for moment resistance and under 0.05 for initial stiffness may indicate an acceptable results dispersion. In addition, the higher dispersion of results was registered for model "B" and may be attributed to the, previously referred, problem with columns with thick flanges leading to unrealistically web thickness.

4. Conclusions

The main conclusions of this study are:

1. The use of a model where the effect of the column radius in shell FEM overall behaviour is neglected seems to lead to lower bending moment resistance values when compared with models considering its effect by increasing the thickness of the web near the flanges or using inclined elements linking column web and flanges. Therefore, it may indicate that the contribution of the column radius could not be neglected to model the joint's overall behaviour with numerical shell FEM. Furthermore, the calculation of an equivalent thickness to use in the column web areas near the column flanges to model the column radius may be carried out carefully when dealing with profiles with thick flanges due to the shell elements overlap that may affect the joint behaviour.
2. The use of inclined elements linking the web and the flanges of the column to simulate the effect of the root radius of the column in shell FEM seems to provide closer behaviour when compared to solid FEM for both moment-resistance and initial stiffness with mean difference values under 3%. Therefore, the use of shell FEM to simulate the moment-rotation behaviour of on-sided internal beam-to-column joints with hot-rolled open sections may be acceptable, and lead to moment resistances and initial stiffness values that may be comparable to solid.
3. Due to the relatively restricted scope of this study, the conclusions and results provided may be interpreted as a guideline for future development. A more comprehensive research should be performed to cover a larger scope: two-sided joints, the use of horizontal and/or vertical stiffeners, the consideration of more levels of axial force (for instance 30 and 70% of the axial column plastic resistance), the consideration of an improved model B avoiding the problems verified for columns with thick flanges, and the use of other moment resistance criteria beyond the 5% plastic strain.

Acknowledgments

This work was partly financed by FCT / MCTES through national funds (PIDDAC) under the R&D Unit Institute for Sustainability and Innovation in Engineering Structures (ISISE), under reference UIDB / 04029/2020, and under the Associate Laboratory for Advanced Manufacturing and Intelligent Systems (ARISE) under reference LA/P/0112/2020. The work is also financed by ga rant with reference UP2021-035 (RD 289/2021) from "Ministerio de Universidades de España", funded by Ethe European Union, NextGenerationEU, attributed to Jorge Conde.

References

[1] A. Corman, “Characterization of the full non-linear behaviour up to the failure of the sheared panel zone under monotonic loading conditions,” 2022.

[2] O. S. Bursi and J. P. Jaspart, “Benchmarks for finite element modelling of bolted steel connections,” *Journal of Constructional Steel Research,* vol. 43, pp. 17-42, July 1997.

[3] O. S. Bursi and J. P. Jaspart, “Basic issues in the finite element simulation of extended end plate connections,” *Computers & Structures,* vol. 69, pp. 361-382, November 1998.

[4] O. Doerk, W. Fricke and C. Weissenborn, “Comparison of different calculation methods for structural stresses at welded joints,” *International Journal of Fatigue,* vol. 25, pp. 359-369, May 2003.

[5] A. J. Sadowski and J. M. Rotter, “Solid or shell finite elements to model thick cylindrical tubes and shells under global bending,” *International Journal of Mechanical Sciences,* vol. 74, pp. 143-153, September 2013.

[6] CEN, *prEN 1993-1-14. Eurocode 3: Design assited by finite element analysis. part 1-14,* 2023.

[7] S. Jordão, “Comportamento de juntas soldadas em nó interno com vigas de diferentes alturas e aço de alta resistência (in Portuguese),” 2008.

[8] in St. Louis, Washington University, *ABAQUS Analysis User's Manual (v6.6) 23.6.1 Shell elements: overview,* 2009b.

[9] R. Ma, L. Yu, H. Zhang, L. Tan, M. Ismail, J. F. Ma and J. Cai, “Experimental and numerical appraisal of steel joints integrated with single- and double-angles for transmission line towers,” *Thin-Walled Structures,* vol. 164, pp. 107833-107833, July 2021.

[10] in St. Louis, Washington University, *ABAQUS Analysis User's Manual (v6.6) 22.1.1 Solid (continuum) elements,* 2009a.